Afro-Asian Journal of Scientific Research (AAJSR)
المجلة الأفروآسيوية للبحث العلمي (AAJSR)
E-ISSN: 2959-6505
Volume 3, Issue 2, April - June 2025
Page No: 70-79
Website: https://aajsr.com/index.php/aajsr/index
SJIFactor 2024: 5.028 ISI 2024: 0.580 معامل التأثير العربي (AIF) 2023: 0.51

The Impacts of Methane (CH_4) on Misrata Municipality's Eco Environment

Mustafa Mahjoub [1*], Giuma Ali Shneba [2], Mustafa Eroba [3], Mohamed Eroba [4], Ali Alabyed [5]
[1] Faculty of Engineering, Misurata University, Misurata, Libya
[2] Mechanical Engineering Department, Higher institute of industrial technology, Alnajilh, Libya
[3] Libyan Academy, Misrata, Libya
[4,5] Faculty of Engineering, Misurata University, Misurata, Libya

تأثير غاز الميثان (CH_4) على البيئة البيئية لبلدية مصراتة

مصطفى مخزوم المحجوب [1*]، د. جمعة علي شنيبة [2]، مصطفى امحمد الربع [3]، محمد مصطفى الربع [4]، علي جمال الأبيض [5]
[1] كلية الهندسة، جامعة مصراتة، مصراتة، ليبيا
[2] قسم الهندسة الميكانيكية، المعهد العالي للتقنية الصناعية، النجيلة، ليبيا
[3] الأكاديمية الليبية، مصراتة، ليبيا
[5،4] كلية الهندسة، جامعة مصراتة، مصراتة، ليبيا

Corresponding author: mosta752911@gmail.com

Received: February 11, 2025	Accepted: April 05, 2025	Published: April 18, 2025

Abstract
The Paper study the Waste disposal that poses significant environmental and health challenges in numerous cities worldwide, including Misrata City. In the absence of effective waste management systems, waste burning has been adopted as an expedient yet unsustainable solution. This study seeks to evaluate the environmental and health impacts of waste incineration in (Saso Mardoum), located south of Misrata, with the aim of highlighting the risks associated with this practice and proposing viable alternatives. The research specifically examines the influence of methane (CH_4) emissions resulting from waste burning on Misrata, assessing the spatial distribution of these emissions and their impact on air quality and the local environment. Computational fluid dynamics software ANSYS was utilized to simulate air flow and gas dispersion, while methane concentration levels in various regions were analyzed to evaluate the degradation of air quality. The findings reveal that waste incineration produces substantial methane emissions, which significantly deteriorate air quality in Misrata. Consequently, the study recommends implementing measures to mitigate waste burning and transitioning to more environmentally sustainable waste disposal practices.

Keywords: Waste disposal, Waste incineration, Methane emissions, Air quality, Environmental and Health impact, Computational fluid dynamics, Gas dispersion, Misrata City.

الملخص:
تدرس الورقة التخلص من النفايات الذي يشكل تحديات بيئية وصحية كبيرة في العديد من المدن في جميع أنحاء العالم، بما في ذلك مدينة مصراتة. وفي غياب نظم فعالة لإدارة النفايات، اعتُمد حرق النفايات كحل مناسب ولكنه غير مستدام. تسعى هذه الدراسة إلى تقييم الآثار البيئية والصحية لحرق النفايات في (ساسو مردوم)، الواقعة جنوب مصراتة، بهدف تسليط الضوء على المخاطر المرتبطة بهذه الممارسة واقتراح بدائل قابلة للتطبيق. يبحث البحث على وجه التحديد في تأثير انبعاثات الميثان (CH_4) الناتجة عن حرق النفايات في مصراتة، وتقييم التوزيع المكاني لهذه الانبعاثات وتأثيرها على جودة الهواء والبيئة المحلية. تم استخدام برنامج ديناميكيات السوائل الحسابية ANSYS لمحاكاة تدفق الهواء وتشتت الغاز، بينما تم تحليل مستويات تركيز الميثان في مناطق مختلفة لتقييم تحلل جودة الهواء. تكشف النتائج أن حرق النفايات ينتج عنه انبعاثات كبيرة

من غاز الميثان، مما يؤدي إلى تدهور كبير في جودة الهواء في مصراتة. وبالتالي، توصي الدراسة وتنفيذ تدابير للتخفيف من حرق النفايات والانتقال الي ممارسات أكثر استدامة بيئياً للتخلص من النفايات.

الكلمات المفتاحية: التخلص من النفايات، حرق النفايات، انبعاثات الميثان، جودة الهواء، التأثير البيئي والصحي، ديناميكيات السوائل الحاسوبية، تشتت الغاز، مدينة مصراتة.

Introduction

Methane (CH_4) is a potent greenhouse gas that poses a significant threat to global and local environmental stability, with a global warming potential more than 80 times greater than that of carbon dioxide over a 20-year period. In the context of Misrata Municipality, located in northwestern Libya, the ecological impacts of methane emissions are increasingly evident due to growing urbanization, industrial activities, and inadequate waste management systems. The region faces challenges stemming from uncontrolled methane release originating from sectors such as agriculture, oil and gas operations, and municipal solid waste. These emissions contribute not only to climate change but also to the degradation of air quality, the disruption of local ecosystems, and heightened public health risks. Understanding the sources, consequences, and potential mitigation strategies related to methane emissions is critical for safeguarding Misrata's environmental integrity and ensuring sustainable development in the face of evolving environmental pressures. Primary Reasons for Waste Incineration can be pointed as following:

- Lack of Waste Management Systems: The absence of efficient waste management systems often forces communities to resort to quick and unsustainable solutions such as incineration [1].
- Rapid Waste Disposal: Incineration is viewed as a fast way to dispose of large quantities of waste, especially in densely populated areas [2].
- Separation of Combustible Materials: Waste is sometimes incinerated to separate combustible materials from non-combustible ones for potential reuse [3].
- Heating: In some regions, waste incineration is employed as a source of heating [4].

Negative Impacts of Waste Incineration:

- **Air Pollution** [5]**:**
  - Waste incineration releases a variety of toxic gases, including carbon dioxide (CO_2), methane (CH_4), nitrogen oxides (NO_x), dioxins, and furans.
  - These gases contribute to global warming and climate change and increase the risk of respiratory diseases such as asthma and bronchitis.
  - Furthermore, they are linked to chronic conditions such as cardiovascular diseases and cancer.
- **Water Pollution** [6]**:**
  - Pollutants from waste incineration can leach into groundwater and surface water, contaminating water sources and making them unfit for drinking or other uses.
  - Water pollution also impacts aquatic life, leading to the degradation of aquatic ecosystems.
- **Soil Contamination** [8]**:**
  - Toxic ash from waste incineration accumulates in the soil, rendering it unsuitable for agriculture and diminishing its fertility.
  - Contaminants from the soil can also infiltrate groundwater, exacerbating water pollution issues.
- **Impact on Public Health** [9]**:**
  - Exposure to air pollutants from waste incineration elevates the risk of respiratory diseases, cardiovascular disorders, cancer, and neurological conditions.
  - Children are particularly vulnerable to these pollutants, facing increased risks of respiratory diseases and developmental issues.
- **Environmental Impact** [10]**:**
  - Waste incineration deteriorates the quality of air, water, and soil, disrupting biodiversity and destabilizing ecosystems.
  - It also contributes to climate change, exacerbating global warming.

The practice of waste incineration, while often employed as a waste management strategy, poses significant and multifaceted environmental and public health risks. It contributes substantially to air pollution through the release of hazardous gases such as methane, carbon dioxide, nitrogen oxides, and dioxins, which not only accelerate global warming but also threaten human respiratory and cardiovascular health. In addition, incineration leads to the contamination of vital natural resources—pollutants infiltrate water bodies, endangering aquatic ecosystems and making water unsafe for human use, while toxic ash degrades soil quality and agricultural productivity. These environmental degradations are compounded by serious public health concerns, particularly for vulnerable populations such as children. Ultimately, the ecological damage and health hazards linked to waste incineration highlight the urgent need for sustainable waste management alternatives that prioritize environmental preservation and human well-being.

Simulation Model

A three-dimensional model was developed to represent the area under study for gas dispersion analysis. The dimensions of the model were set at 45 km in length, 1 km in width, and 300 meters in height, with the emission source area clearly defined. Moreover, the model was divided into smaller elements (mesh) of varying sizes (10 meters, 20 meters, and 30 meters) to evaluate the effect of element size on the accuracy of the results. Next, boundary conditions were specified, including wind speed and gas concentration at the inlet and outlet of the region. Additionally, initial flow conditions, such as velocity, pressure, and gas concentration, were established at the start of the simulation [11].

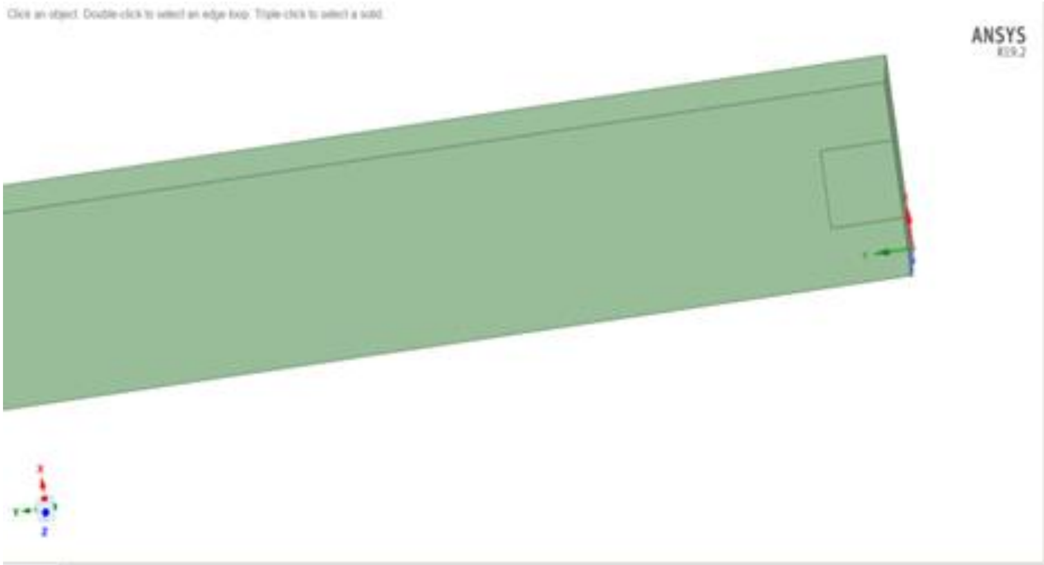

Figure 1: Area of Study.

Table 1 presents a comparative overview of the mesh densities for three computational models, highlighting significant variations in the number of nodes and elements. Model One features the highest resolution, with over 14 million nodes and 13 million elements, indicating a highly detailed and computationally intensive simulation likely used for precise analyses. Model Two offers a moderate mesh density, balancing accuracy and efficiency with approximately 1.8 million nodes and 1.6 million elements.

Table 1: The number of nodes and elements for the three models were as follows:

	Model One	Model Two	Model Three
Nodes	14089500	1836816	565565
Elements	13497000	1687500	499120

In contrast, Model Three employs the coarsest mesh, consisting of around 565,000 nodes and 499,000 elements, suitable for preliminary or large-scale studies with lower computational demands. The data underscores a trade-off between model accuracy and computational cost, guiding the appropriate selection of model complexity based on specific simulation objectives. In this direction, the governing equations were solved using the computational fluid dynamics (CFD) software ANSYS, with the activation of the k-epsilon 2 equation model. The solution process was iterated until a stable solution was achieved [11].

Results and Discussion

In term of results and discussion, Figure 2 illustrates the convergence behavior of the First Model by showing the variation of residuals over 500 iterations. Initially, the residuals display significant oscillations, particularly in the first 50–75 iterations, as the solver adjusts from the initial conditions. Over time, most residuals decrease steadily and stabilize, with several falling below the threshold of 1e-06—an indication of satisfactory numerical convergence. However, a few residuals remain at slightly higher values (around 1e-03 to 1e-04), suggesting slower convergence for certain equations, possibly due to complex flow features or boundary conditions. Overall, the plot confirms that the simulation achieved a stable and reliable solution, validating the effectiveness of the model setup and mesh density.

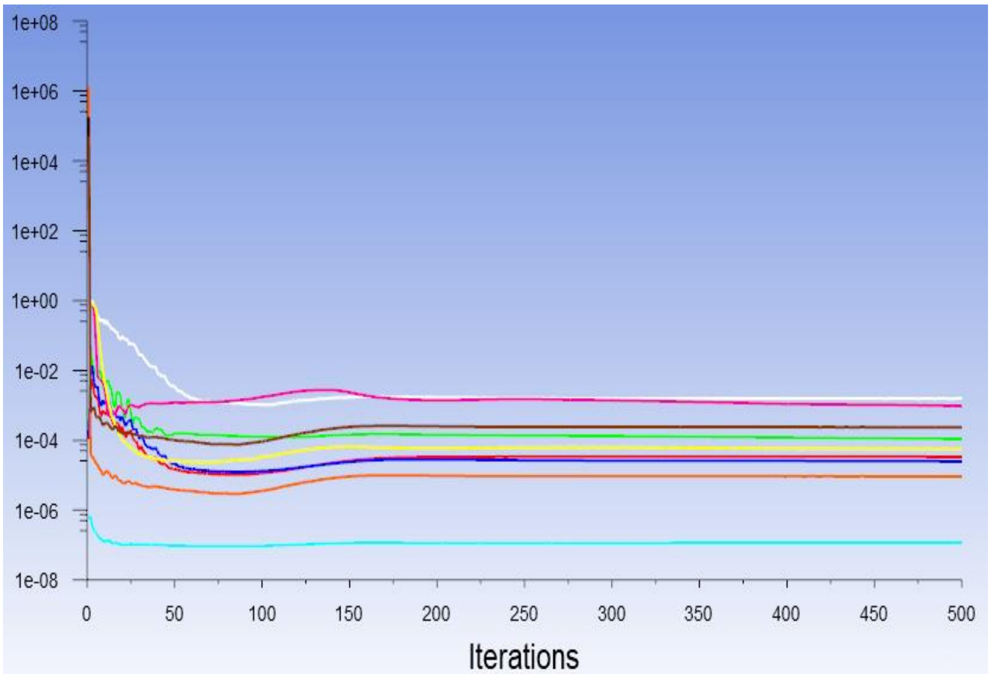

Figure 2: Calculated Values and Residual Values for the First Model.

Figure 3 presents the residual convergence behavior of the Second Model, showing a rapid and stable decline in residuals within the first 100 iterations. This suggests that the model achieved efficient numerical convergence, likely aided by its lower mesh density compared to the First Model. Most residuals stabilize below 1e-06, indicating a satisfactory solution for key variables, while a few remain around 1e-03 to 1e-04, reflecting slower convergence for certain components, possibly due to solver settings or complex flow characteristics. Overall, the Second Model demonstrates strong computational efficiency and reliable performance, making it suitable for simulations requiring a balance between accuracy and speed.

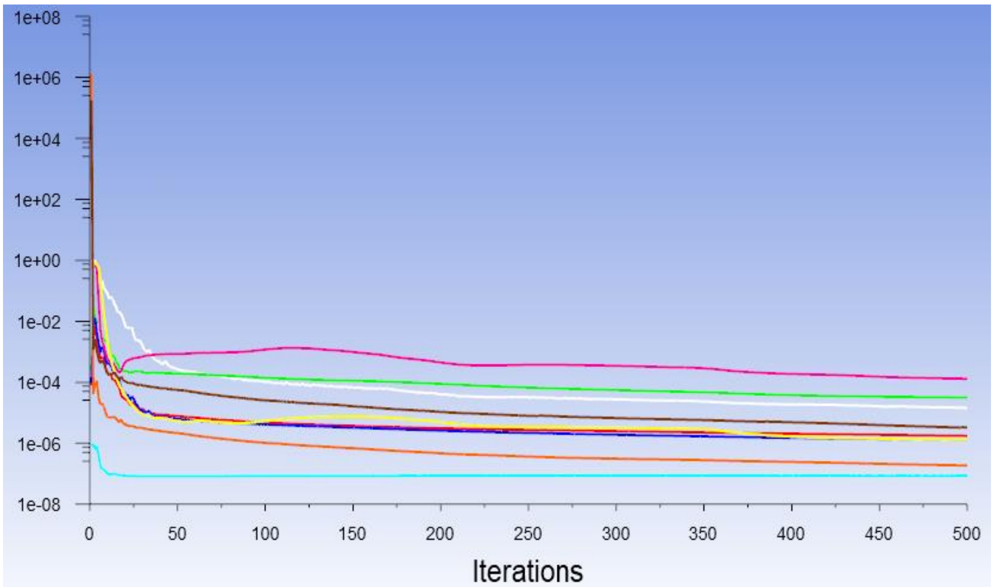

Figure 3: Calculated Values and Residual Values for the Second Model.

Figure 4 illustrates the contour plot of calculated values for the Third Model, likely representing a scalar field such as temperature, velocity magnitude, or pressure distribution. The color gradient, ranging from deep blue to red, indicates varying intensities, with the red zone suggesting a region of maximum value—possibly a high-stress concentration, heat source, or flow acceleration zone—while the blue regions signify lower intensity or equilibrium zones.

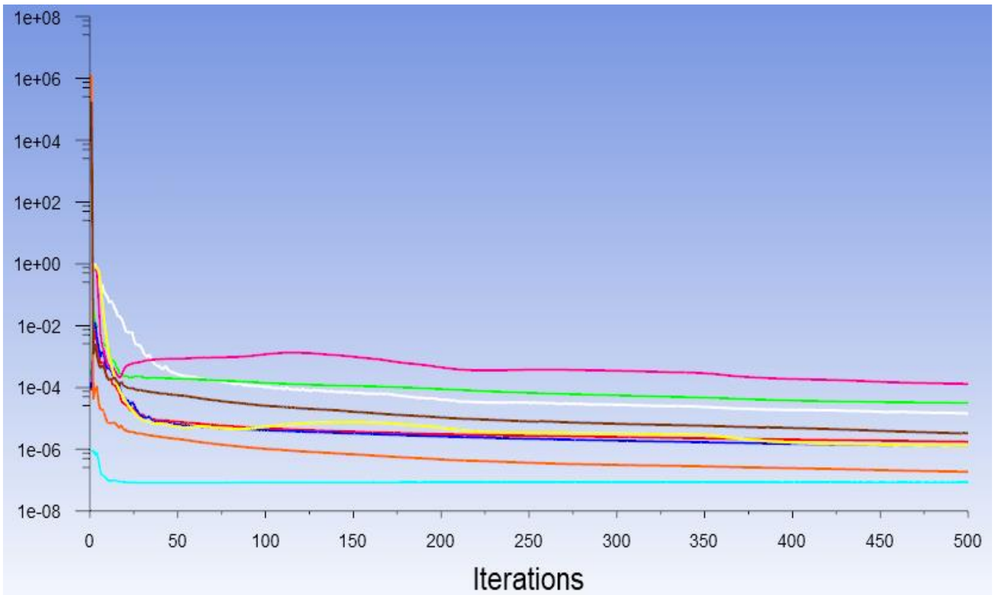

Figure 4: Calculated Values and Residual Values for the Third Model.

The symmetrical pattern and smooth transition of contours reflect a stable and physically consistent solution, implying that the Third Model, despite its coarser mesh as shown in Table 1, is capable of capturing essential flow or field characteristics. This visualization confirms the model's effectiveness in resolving the dominant behavior of the system, although finer details may be better captured in higher-resolution models. Three horizontal levels were established at distances of 42 km, 43 km, and 44 km from the waste emission source, along with three vertical levels at heights of 10 m, 20 m, and 30 m above the ground surface [11].

Figures 5 through 13 present the gas concentration distributions across three vertical levels for each of the three models. In the First Model (Figures 5–7), gas concentration patterns show detailed spatial variation, likely due to the model's high mesh density, enabling fine-resolution depiction of gradients. The Second Model (Figures 8–10) exhibits similar distribution trends but with slightly less detail, reflecting its moderate mesh resolution. Finally, the Third Model (Figures 11–13) reveals a more generalized concentration profile, with less pronounced gradients, consistent with its coarser mesh. Overall, the comparison across models and levels highlights how mesh resolution influences the accuracy and clarity of gas dispersion simulations, with the First Model offering the most refined visualization and the Third Model providing a more computationally efficient, yet less detailed, representation.

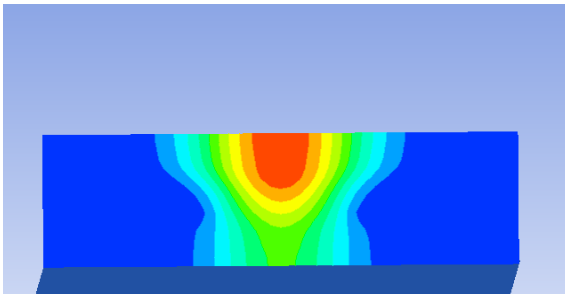

Figure 5: Gas Concentration at the First Level of the First Model.

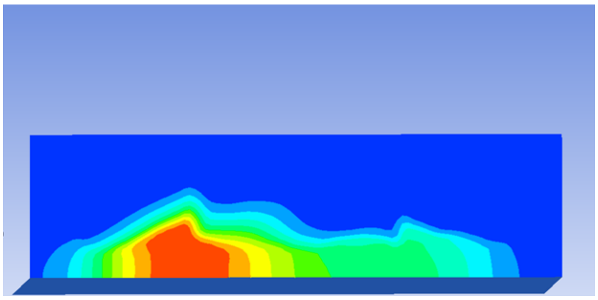

Figure 6: Gas Concentration at the Second Level of the First Model.

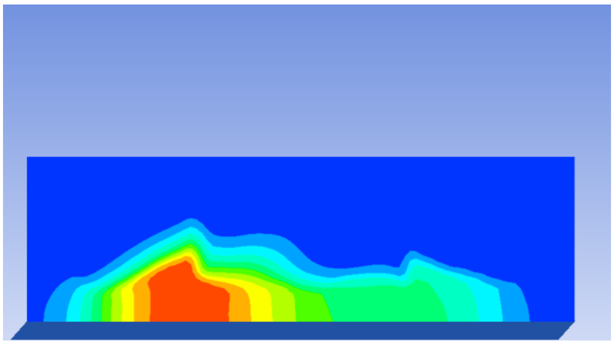

Figure 7: Gas Concentration at the Third Level of the First Model.

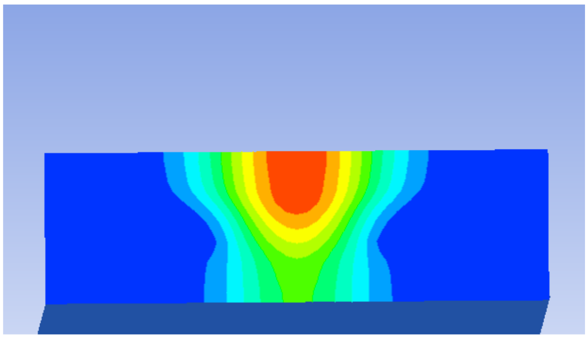

Figure 8: Gas Concentration at the First Level of the Second Model.

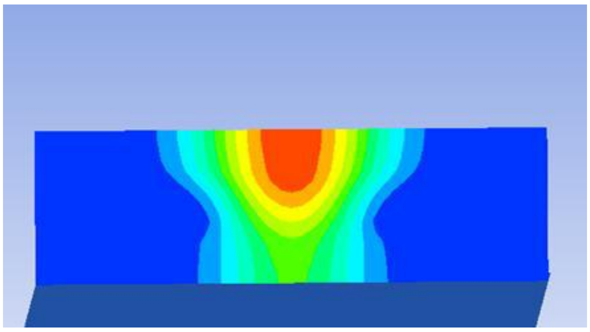

Figure 9: Gas Concentration at the Second Level of the Second Model.

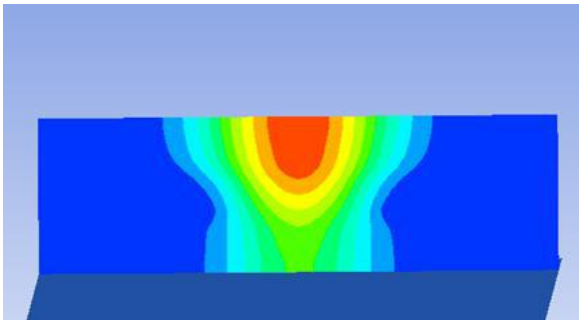

Figure 10: Gas Concentration at the Third Level of the Second Model.

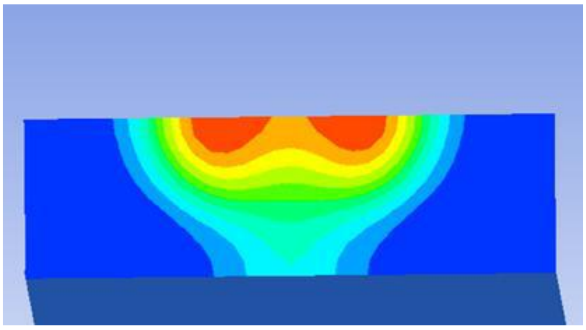

Figure 11: Gas concentration at the first level of the model Three.

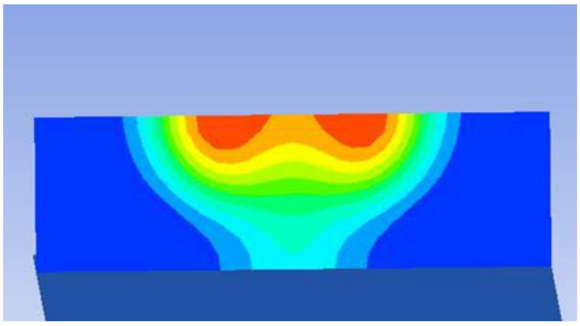

Figure 12: Gas concentration at the second level of the model Three.

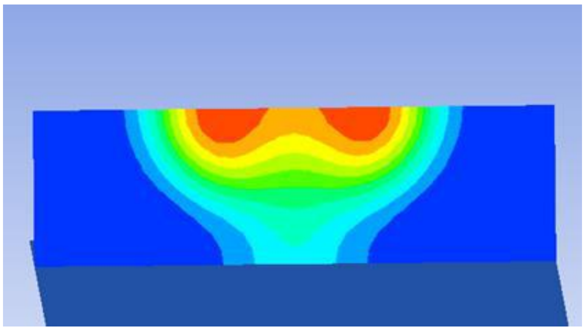

Figure 13: Gas concentration at the third level of the model Three.

Figures 14 through 22 illustrate the gas concentration distribution along the vertical Z-axis at three levels for each of the three models. In Model One (Figures 14–16), the concentration profiles demonstrate high spatial resolution, capturing fine vertical gradients and subtle variations due to the model's dense mesh. Model Two (Figures 17–19) maintains a similar overall pattern but with slightly reduced detail, indicative of its intermediate mesh complexity. In contrast, Model Three (Figures 20–22) displays a more smoothed and generalized concentration profile along the Z-axis, aligning with its coarser mesh structure. This vertical analysis emphasizes how mesh resolution impacts the ability to accurately resolve gas dispersion behavior in the vertical plane, with Model One offering the highest fidelity, followed by Model Two and Model Three in terms of representational precision and computational efficiency.

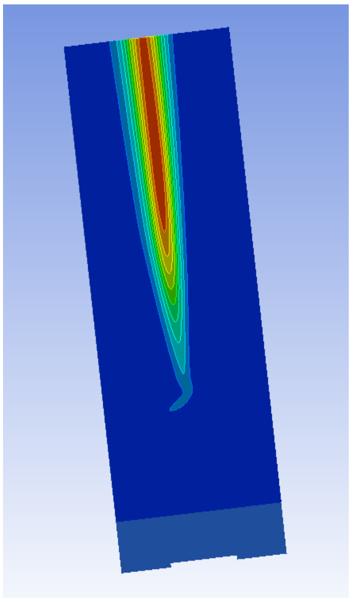

Figure 14: Gas concentration at the first level of Model One.

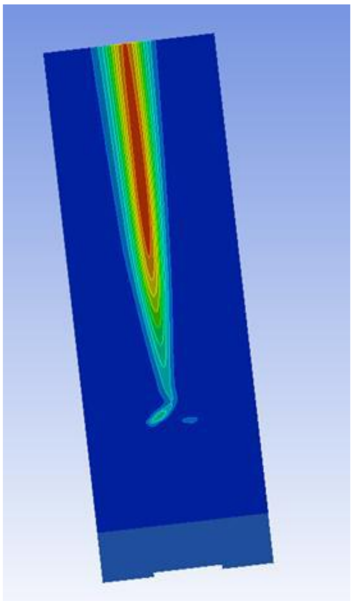

Figure 15: Gas concentration at the second level of the Model One.

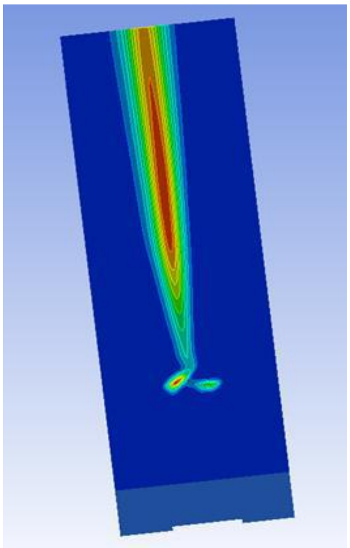

Figure 16: Gas concentration at the third level of the Model One.

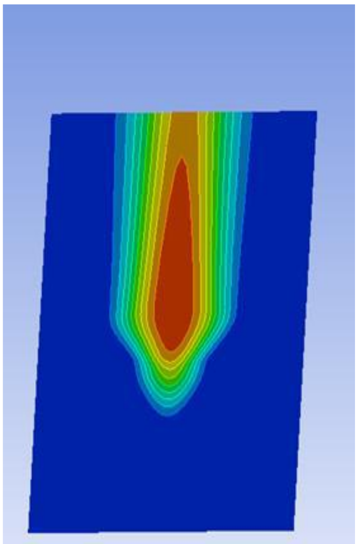

Figure 17: Gas concentration at the first level of Model Two.

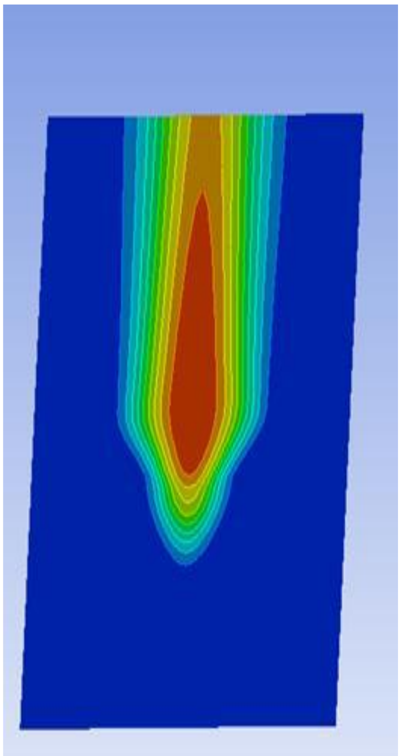

Figure 18: Gas concentration at the second level of the Model Two.

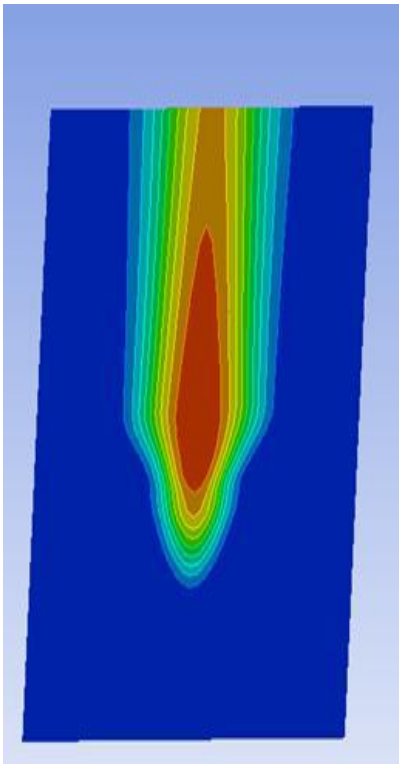

Figure 19: Gas concentration at the third level of Model Two.

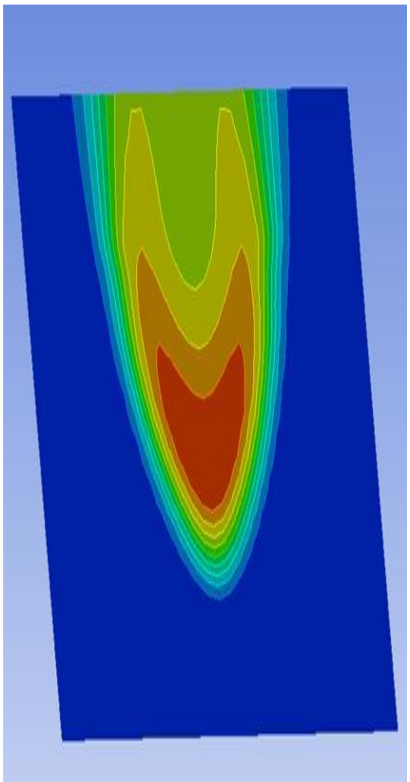

Figure 20: Gas concentration at the first level of the Model Three.

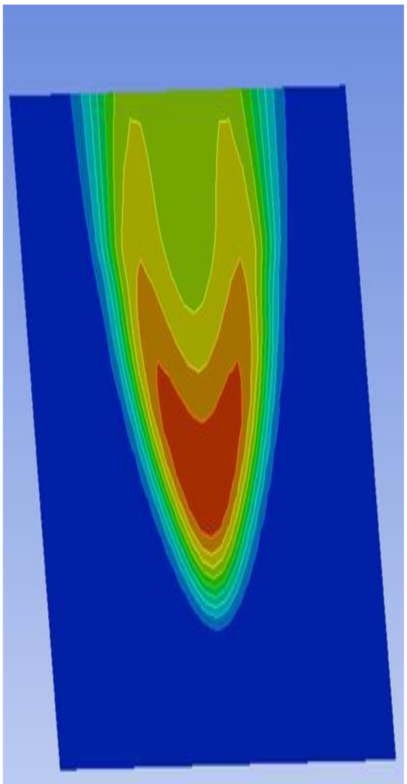

Figure 21: Gas concentration at the second level of the Model Three.

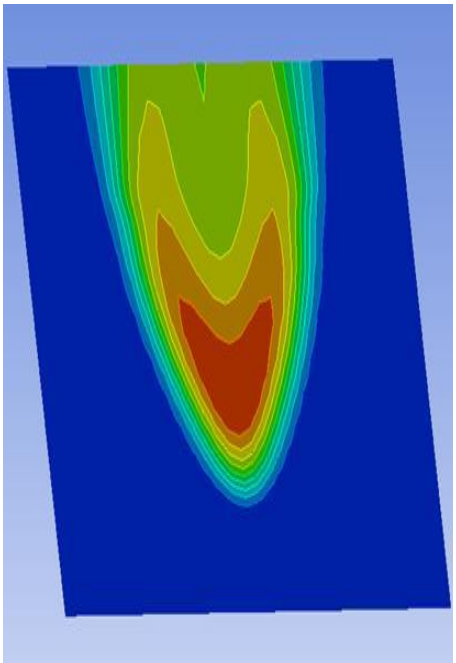

Figure 22: Gas concentration at the third level of the Model Three.

Conclusion

Building upon the previously identified methane concentration levels, Dalton's Law of Partial Pressures was applied, which states that the total pressure of a gas mixture equals the sum of the partial pressures exerted by each individual gas component within the mixture.

$$\rho = (m\%_{air} * \rho_{air}) + \left(m\%_{CH_4} * \rho_{CH_4}\right) + (m\%_{NO} * \rho_{NO})$$

- The concentration of CH4 under the worst conditions was found to be 0.155332% [11].
- The results obtained from Dalton's Law yielded a value of 187.5 ppm [11].
- According to the World Health Organization (WHO), the permissible and safe levels of methane for humans' range between 1.7 and 1.9 ppm [7].
- In the application of Dalton's formula, it is important to note that the experimental study was conducted for two gases, Methane (CH_4) [11].

Based on the analysis of methane concentrations obtained from simulation results, Dalton's Law of Partial Pressures was applied to assess the total pressure exerted by the gas mixture, incorporating the individual contributions from air, methane (CH_4), and nitrogen oxide (NO). The concentration of methane under the worst-case scenario was determined to be 0.155332%, which, when processed through Dalton's formula, yielded a methane partial pressure equivalent to 187.5 ppm. This value far exceeds the World Health Organization's (WHO) recommended safe exposure range of 1.7 to 1.9 ppm for humans. Although the experimental evaluation primarily considered methane, the results clearly indicate a critical health risk due to elevated concentrations. Consequently, the study underscores the significant environmental and health implications of methane exposure in the modeled conditions, highlighting an urgent need for mitigation strategies and adherence to international air quality standards.

Symbols:

Symbol	Geometric Meaning	Unit of Measurement
-	Methan Gas	CH_4
kg/m^3	Density	ρ
kg/m^3	Air Density	ρ_{air}
kg/m^3	Density of Nitrogen Oxide Gas	ρ_{NO}
kg/m^3	Density of Methane Gas	ρ_{CH_4}
-	Mass Fraction of Air	$m\%_{air}$
-	Mass Fraction of Nitrogen Oxide Gas	$m\%_{NO}$
-	Mass Fraction of Methane Gas	$m\%_{CH_4}$
-	Parts Per Million (ppm)	ppm
-	Meter	m

-	Kilometer	Km
-	Square Meter	m^2
-	Meter/Second	m/s

References

1. Feng, Z., & Kobayashi, K. (2009). Assessment of the impact of NO2 on vegetation in East Asia. *Journal of Forestry Research, 20*(1), 1–8.
2. Fangmeier, A., & Müller, H. (2010). The effects of nitrogen dioxide on vegetation: Results from field experiments. *Environmental Pollution, 3*(3), 155–169.
3. Zhang, W., & Feng, Z. (2010). Nitrogen dioxide (NO2) phytotoxicity and the decay of epiphyllous lichens. *Environmental Pollution, 158*(3), 996–1002.
4. IPCC. (2014). *Climate Change 2014: Impacts, Adaptation, and Vulnerability*. Cambridge University Press.
5. Lan, W., Zhang, X., Li, Y., & Wang, J. (2015). Methane: A review on sources and environmental hazards. *International Journal of Environmental Science and Development, 6*(5), 358–366.
6. Smith, W. H. (2015). Effects of carbon dioxide enrichment on plant growth. *Journal of Applied Botany and Food Quality, 88*, 1–10.
7. World Health Organization. (2021). *Soil pollution: A global overview of causes, impacts, and solutions* (Report No. WHO/ENV/21). https://www.who.int/...
8. United Nations Environment Programme. (2021). *Soil pollution: Causes, effects, and solutions* (Report No. UNEP/ENV/21/003). https://www.unep.org/...
9. Brown, K., & White, M. (2022). Effects of heavy metal deposition in soil due to incineration emissions. *Environmental Pollution Journal, 30*(4), 312–325.
10. Ruckerl, R., Schneider, A., Breitner, S., Cyrys, J., & Peters, A. (n.d.). *Health effects of particulate air pollution: A review of epidemiological evidence* [Unpublished manuscript]. Helmholtz Zentrum München.
11. CFD Online. (n.d.). *Wiki main page*. Retrieved from http://www.cfd-online.com/wikimainpage